Computational fluid dynamic study on effect of Carreau-Yasuda and Newtonian blood viscosity models on hemodynamic parameters

Nitesh Kumar[a], Abdul Khader[a], Raghuvir Pai[a,*], Panayiotis Kyriacou[b], Sanowar Khan[b] and Prakashini Koteshwara[c]

[a]*Department of Mechanical and Manufacturing Engineering, Manipal Institute of Technology, Manipal Academy of Higher Education, Manipal, India*

[b]*School of Mathematics, Computer Science and Engineering, Department of Electrical and Electronic Engineering, University of London, London, UK*

[c]*Department of Radiodiagnosis, Kasturba Medical College and Hospital, Manipal Academy of Higher Education, Manipal, India*

Abstract. Pulsatile blood flow through the human carotid artery is studied using Computational Fluid Dynamics (CFD) in order to investigate the effect of blood rheology on the hemodynamic parameters. The carotid artery model used is segmented and reconstructed from the Magnetic Resonance Images (MRI) of a specific patient. The results of a non-Newtonian (Carreau-Yasuda) model and a Newtonian model are studied and compared. The results are represented for each peak systole where it is observed that there is significant variation in the spatial parameters between the two models considered in the study. Comparison of local shear stress magnitude in different branches namely Common Carotid Artery (CCA), Internal Carotid Artery (ICA) and External Carotid Artery (ECA) show that the shear thinning property of blood influences the Wall Shear Stress (WSS) variation. This is observed in branches where there is reduction in diameter and where the diameter reduces due to plaque deposition and also in the region where there is flow recirculation like carotid sinus.

Keywords: Carotid artery, computational fluid dynamic, Newtonian and Carreau-Yasuda, wall shear stress

1. Introduction

THE carotid arteries are the blood vessels which supply blood to the brain, which originate from the aorta as Common Carotid Artery (CCA) and near the plane of the throat the carotid artery branches into Internal Carotid Artery (ICA) and External Carotid Artery (ECA). The ICA supplies blood to the brain and the ECA supplies blood to the face and neck. There are two carotid arteries one in the left side of the neck named as Left Carotid Artery and one in the right as Right Carotid Artery. At the region

*Corresponding author: Raghuvir Pai, Department of Mechanical and Manufacturing Engineering, Manipal Institute of Technology, Manipal Academy of Higher Education, Manipal, India. Tel.: +91 99 4567 0697; E-mail: raghuvir.pai@manipal.edu.

where the CCA bifurcates, the vessels enlarge to form a unique bulb named as carotid sinus. Stenosis in the carotid artery is the root cause of about 80% of strokes [1]. Deposit of plaque are generally soft structures which forms an arbitrary and irregular area inside the arteries. Here platelets fill the cracked irregular areas forming blood clots in the artery or its branches causing atherosclerosis. The most favorable location for the deposition of atherosclerotic plaque is at the bifurcation zone and the inner curvature of the vasculature, also they localize at the regions of low Wall Shear Stress (WSS) [2]. High WSS is protective towards atherosclerosis formation while the region of low WSS is prone to atherosclerosis. Therefore, the initiation of thickening of the arterial wall begins at the region of low WSS [3–7]. Known dynamic viscosity of blood and blood velocities are multiplied to calculate the WSS. Velocities are generally calculated using CFD techniques in solving the Navier stokes equation by iterative methods. However, CFD require accurate boundary conditions, computational time and clinical expertise. Alternately, blood velocities can be obtained by phase contrast MRI (PC-MRI) technique. It was observed that PC-MRI technique underestimates the velocity and WSS magnitude due to lack of spatial resolution [8]. However, qualitatively both MRI and CFD are similar. Local hemodynamic parameters are governed by both pulsatile pressure, bifurcation geometry along with the properties of the arterial wall and blood rheology [9]. The flow in the carotid artery was studied by many researchers [10–13]. In these studies, blood was modelled as Newtonian fluid and shear thinning characteristics were ignored, arguing that the shear rate in large arteries are high and the blood viscosity was considered equal to high shear rate viscosity limit. Also, some researchers have considered simplified geometries of the realistic arteries for the computational models to simulate blood flow [14,15].

Milner et al. [16] compared idealized and realistic models of carotid artery and found that the idealized model when analyzed masks some key observation which was observed with realistic models. In addition to this, Taylor et al. [17] developed a finite element framework and computational study of vasculature to study clinically relevant blood flow problems and validated the computational results with experimental data and presumed that with good knowledge of the vascular hemodynamic conditions in individual patients and the combination of computational framework a better treatment can be devised in order to improve patient care. Deplano and Siouffi [18] used a stenosed model to study both experimentally and numerically the determination of WSS at the downstream of stenosis using an ultrasonic velocimeter and a finite element package for numerical simulation and found good relation between the two.

For the realistic study of human vasculature, as suggested by researchers, accurate modelling of the vasculature is important. Ladak and Milner [19] developed a rapid extracting technique to extract the arterial geometry from MR images and used Finite element methods to study the hemodynamics of the vasculature. Of all the hemodynamic parameters, carotid artery stenosis severity is a major indicator of risk of stroke. However, if was found that individuals even with severe carotid artery disease do not suffer stroke, whereas strokes occur with individuals having medium or mild stenosis. Local factors along with severity of stenosis plays a major role in predicting the risk of stroke. Steinman et al. [20] investigated the effect of the flow patterns on different carotid artery models with varying stenosis patterns using computational simulations, and found flow patterns provide accurate indications of vulnerable plaques. At post-stenotic regions complex flow separation zones were created depending on the degree of stenosis and oscillations of WSS at the downstream of stenosis, which results in low WSS regions [21]. Computational methods can be an alternative for in vivo measurement techniques like MRI with an aim in obtaining accurate vasculature hemodynamics which can help in identifying the risks of plaque rupture. Stroud et al. [22] studied a endartectomy specimen of carotid bifurcation with varying Reynolds number and pulsatile flow and found high WSS and determined that a suitable turbulence model is required to capture laminar and turbulent behavior of blood flow. Zhao et al. [24] and Marshal et al. [23] used a

combined MR and CFD modelling study for a pulsatile flow in a carotid bifurcation model obtained from MRI scans. Velocities obtained from PCMR (Phase Contrast Magnetic Resonance) were used as boundary conditions and a detailed comparison of velocity patterns were made between CFD and MRI measurements. It was observed that MR measurements were inadequate to portray the secondary flow pattern and hence a combination of MR and CFD was used to obtain a more reliable information about 3-dimensional velocity field. Morbiducci et al. [25] suggested that proper boundary conditions effects the solutions of governing equations of blood flow and investigated the influence of outflow boundary condition assumptions in an image based CFD model of carotid bifurcation. They recommended to adopt more realistic constraints to study the predictions of the outcomes related to alternate therapeutic interventions and the role of local fluid dynamics and other biomechanical factors in vascular diseases.

Blood is a shear thinning fluid and the general Newtonian model will not capture the hemodynamics at critical locations [26]. Johnston et al. [27] studied blood flow through coronary arteries using different non-Newtonian blood viscosity models and concluded that Carreau-Yasuda models gives a better approximation of the WSS at low shear to mid shear range. Chen and Lu [28] investigated the non-Newtonian flow in a bifurcation model to solve the governing equations in which the shear thinning behavior was incorporated by using Carreau-Yasuda model and investigated its influence on the flow phenomena. He found significant differences between Newtonian and the Carreau-Yasuda model and determined that non-Newtonian properties of blood is an important factor in hemodynamics and plays a very important role in vascular biology [28,29].

In the present study, MR images of a patient specific carotid artery is reconstructed using MIMICS. The reconstructed 3D model is exported to ANSYS CFX and the effect of non-Newtonian blood viscosity on the velocity distribution, WSS and shear strain rate in a rigid carotid artery bifurcation model under steady and transient condition is analyzed. The shear thinning property of blood is taken into account using Carreau-Yasuda blood viscosity model and a detailed comparison between Newtonian and non-Newtonian model is presented.

2. Methodology

2.1. Image acquisition and reconstruction

One individual subject was subjected to ultrasound imaging to study the degree of stenosis as a preliminary study. A set of 2D images were acquired with MRI scans in DICOM format and were imported to MIMICS (Materialise, Leuven, Belgium) for image processing. Thresholding was used to classify the pixels with a Hounsfield range of approximately 120–150 and using region growing techniques the geometrical model of the blood vessel is constructed. The generated 3D model is subjected to smoothing to remove any unwanted irregularities in the model due to low resolution in some areas. Finally, the 3D model of the vessel is imported to Ansys 17 for post processing. Figure 1 shows the MRI slices used and reconstructed 3D model.

2.2. Blood flow measurement

Blood flow velocity is measured by acquiring the velocity components at the common carotid artery. The acquired data was synchronized with the cardiac cycle. A slice at the common carotid artery was selected to quantify the flow. After segmenting the lumen of the artery, the velocity wave form was integrated over the lumen inlet. Figure 2 shows the velocity profile at the common carotid artery. This velocity waveform is chosen for delineation of the inlet velocity profile given at the inlet of the computational model.

Fig. 1. MRI image of the carotid artery.

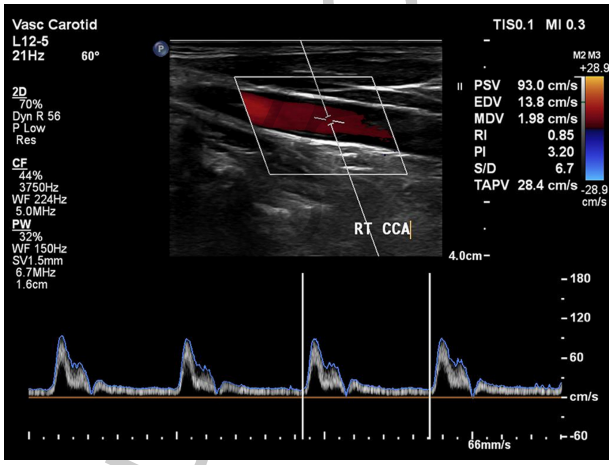

Fig. 2. Ultrasound Doppler image to acquire the velocity profile at the inlet.

2.3. Flow modelling and computational setup

The flow of blood is governed by Navier stokes equation. The conservation of mass and momentum for incompressible fluid in three dimensions is given as

$$\nabla \cdot v = 0 \tag{1}$$

$$\rho\left(\frac{\partial v}{\partial t} + v\nabla v\right) = \nabla P + \nabla \tau \tag{2}$$

where ρ is the constant density, v is the velocity vector, τ is the shear stress tensor. The body forces and energy equations can be ignored if there is no requirement on thermal information. To calculate the blood viscosity, constitutive equations have to be employed. Different constitutive equations are proposed to

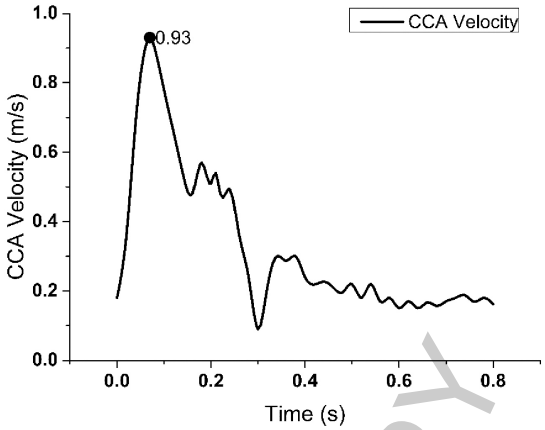

Fig. 3. Inlet Velocity waveform highlighting peak velocity at 0.072 s.

model the flow of blood, but the simplest of them all is the Newtonian model which assumes the viscosity as constant. Recently, many studies have suggested models which incorporate the shear dependence of blood can predict the hemodynamics. Most common of them are power law, Casson and Carreau-Yasuda models [30,31]. The power law is expressed as

$$\mu = k\dot{\gamma}^{n-1} \tag{3}$$

where μ is the apparent blood viscosity k is flow consistency index, n is the power law index which shows the non-Newtonian behavior of the blood and $\dot{\gamma}$ is the shear rate [32]. This model is the simplest one used to represent the non-Newtonian behavior of the fluid. However, it has a range from zero to infinite shear rate and only the values in realistic range will approximate the non-Newtonian behavior. Also, the power law index is usually selected so that the model replicates the shear thinning behavior in hemodynamic simulations [33]. The Casson model takes into account both the shear thinning behavior and the yield stress of blood. However, it is the Carreau-Yasuda model which better fits the shear rate relationship and the experimental data [34].

$$\frac{\mu - \mu_\infty}{\mu_0 - \mu} = (1 + (\lambda\dot{\gamma})^a)^{\frac{n-1}{a}} \tag{4}$$

where $\mu_0 = 0.056$ Pa.s is the viscosity at zero shear rate, $\mu_\infty = 0.0035$ Pa.s viscosity at is the infinite shear rate, $\lambda = 3.313$ s is the relaxation time, power law index $n = 0.3568$ and Yasuda exponent $a = 2$.

The 3D unsteady Navier Stokes equations were solved by implementing a finite volume scheme using ANSYS CFX (ANSYS Inc., Canonsburg, PA). The walls of the carotid artery was considered as rigid with no slip condition. At the inlet, time dependent velocity wave form obtained by Ultrasound Doppler of a patient was prescribed as shown in Fig. 3 which corresponds to the waveform as shown in Fig. 2. For outlets, an impedance method developed by Olufsen [35] and Olufsen et al. [36] was implied by modelling the vascular system as a fractal network. In this method, the vessels beyond the imaging domain are approximated with the help of 1D flow approach [37]. The applied pressure waves on ICA and ECA are shown in Figs 4 and 5. A schematic showing the boundary conditions at the inlet and outlet is shown in Fig. 6.

The simulation was conducted on a computational model of the carotid artery of a 64-year-old male extracted from MR scans. An eccentric partially calcified plaque measuring 1 cm in length and 2.5 mm thick was found in the proximal ICA, without causing any hemodynamically significant stenosis during

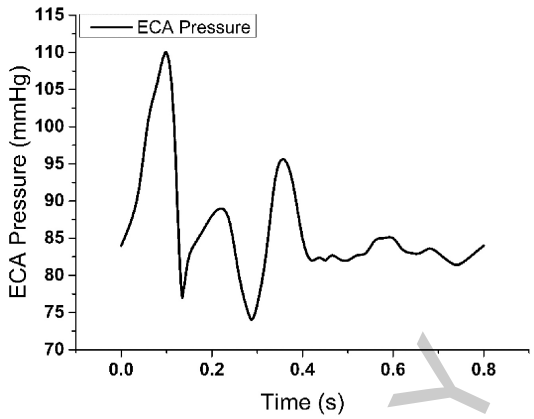

Fig. 4. Outlet pressure waveform at ECA outlet obtained by impedance boundary condition.

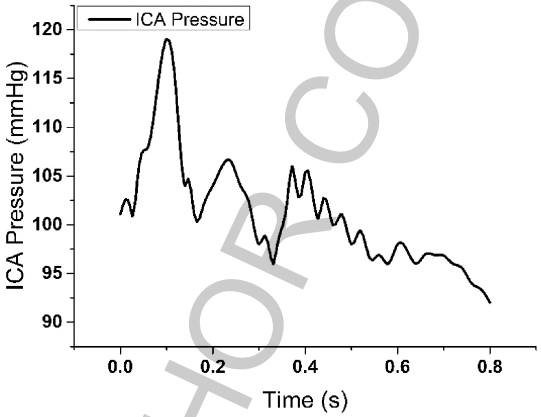

Fig. 5. Outlet pressure waveform at ICA obtained from impedance boundary conditions.

Fig. 6. Carotid artery model showing inlet and outlet boundary conditions.

Ultrasound (US) testing as shown in Fig. 7. The fluid model is discretized into unstructured tetrahedral elements using ICEM CFD as shown in Fig. 8 and Inflation is used to capture the boundary effect with a total thickness of 1 mm as shown in Fig. 9.

3. Results and discussion

In the present study, since the main focus is on the carotid artery, initially a steady state validation is carried out and results obtained are compared with the [38]. The velocity contours obtained are compared

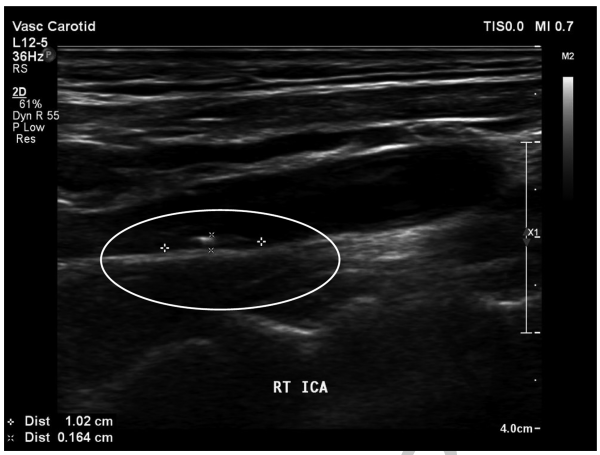

Fig. 7. Ultrasound Doppler scan image showing location and geometry of the eccentric plaque in ICA.

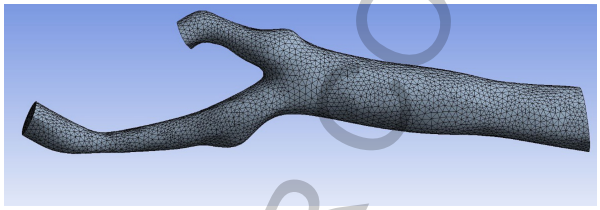

Fig. 8. Finite volume mesh used in the simulation.

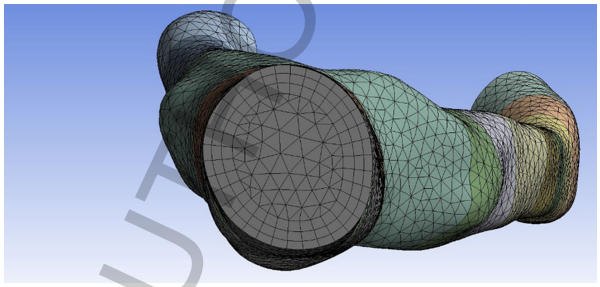

Fig. 9. Inflation at the boundary with 5 layers to capture the boundary effects.

with the literature at the transverse section as shown in the Fig. 10. Accuracy of any numerical simulation primarily depends on quality of the mesh. A good and fine mesh should be able to resolve the velocity vectors and effectively capture the hemodynamics at various regions in the carotid bifurcation used in this study. The grid independence test is performed to check the quality of the mesh for solution convergence by varying the number of control volumes in the computational domain. Grid independency test carried out is shown for carotid bifurcation adopted in the CFD study to validate the numerical simulation with current literature and subject specific carotid bifurcation. A laminar flow model was used to simulate the steady flow in the carotid arteries with RMS value of 10^{-4}. A maximum of 100 iterations was taken for convergence in the study. Less than 0.3% variation can be observed for average WSS for element density of 36500 to 111677 elements. Therefore, based on the grid independence study 36000 elements were used as shown in Fig. 11.

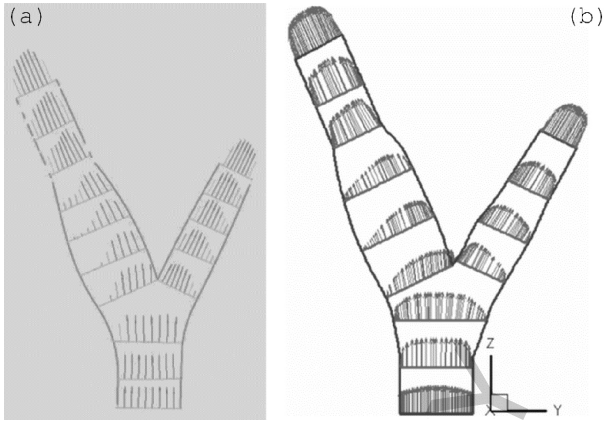

Fig. 10. Comparison of simulated velocity vectors at X-Y Plane with [38], (a) computed Velocity, (b) Literature.

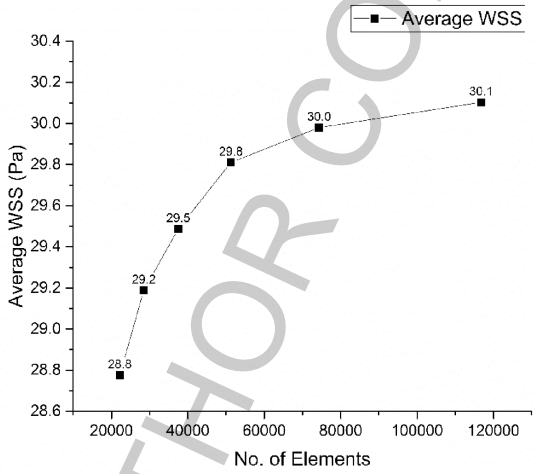

Fig. 11. Grid independence study.

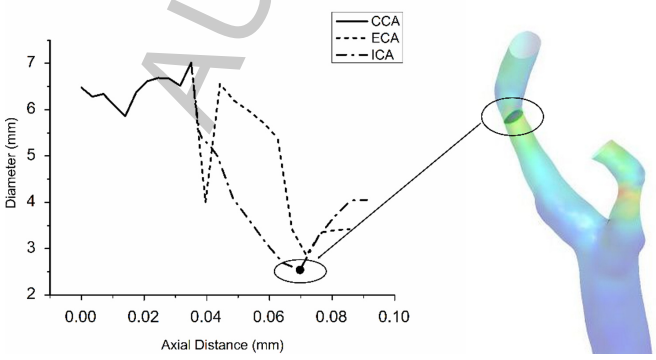

Fig. 12. Variation of Diameter along CCA, ICA and ECA highlighting the location where the diameter is minimum.

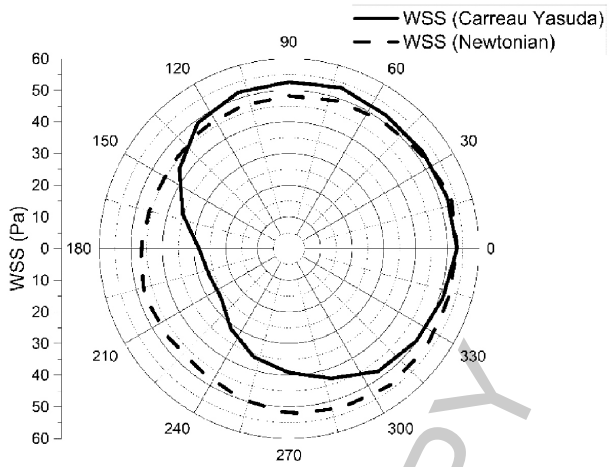

Fig. 13. Variation of WSS at the neck of the stenosis in ICA at peak systole showing the over estimation of WSS.

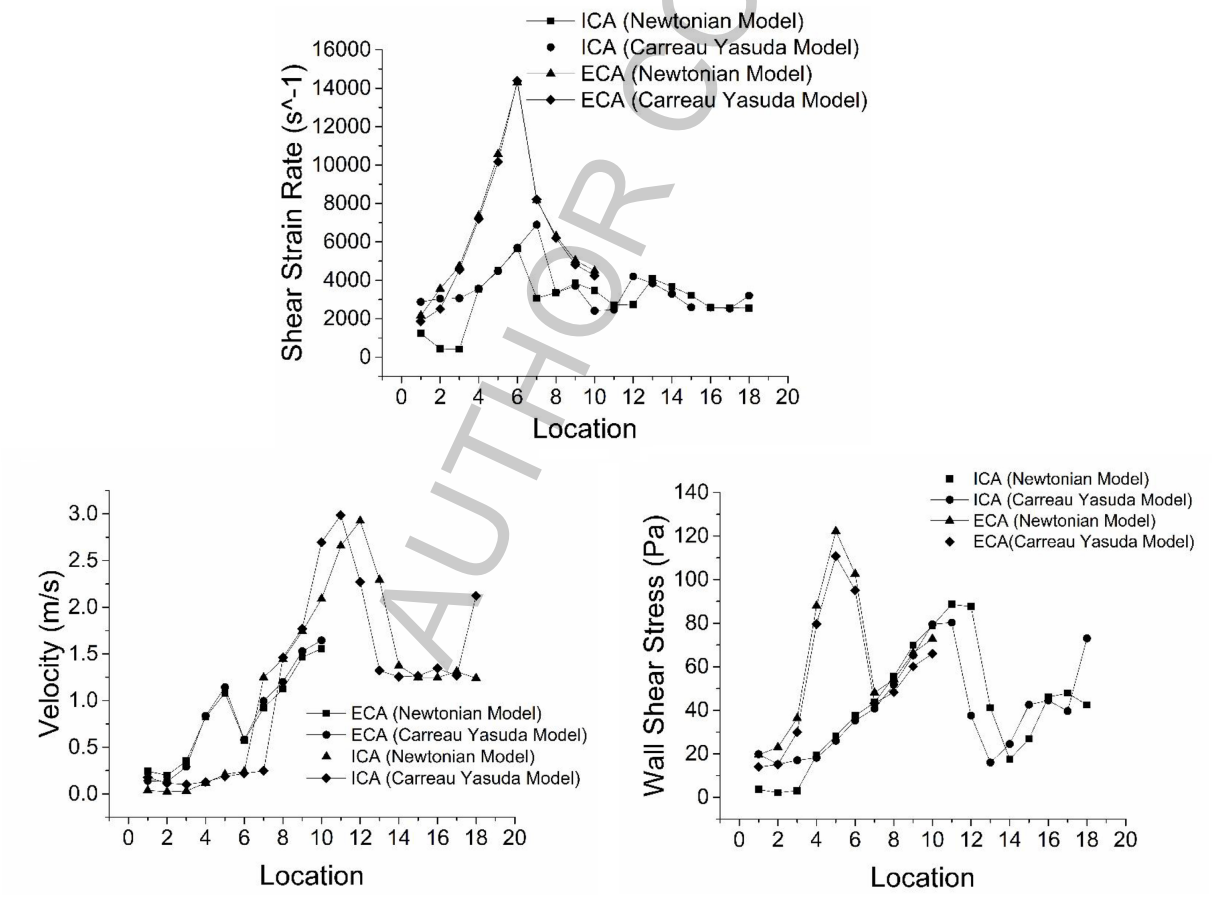

Fig. 14. Variation of shear strain rate, velocity and WSS along the axis of ECA, ICA and CCA.

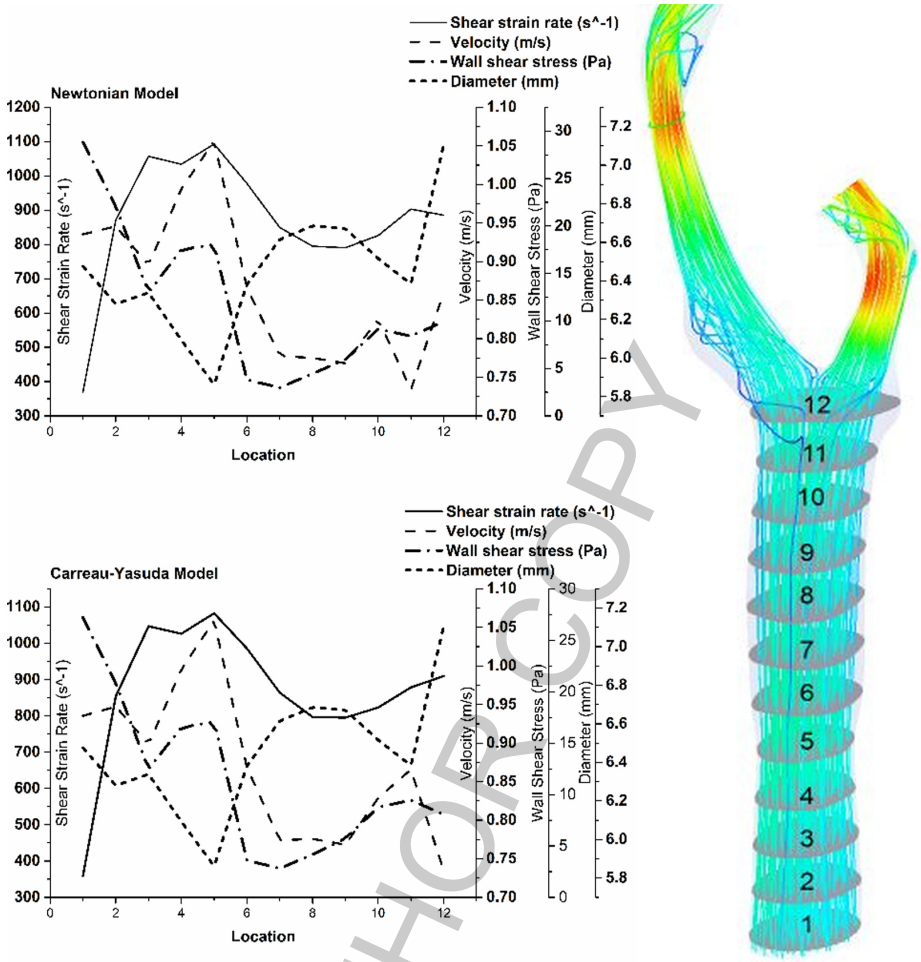

Fig. 15. Variation of Shear strain rate, WSS, Velocity and Diameter along the axis of CCA and its corresponding streamlines highlighting the recirculation zones.

A steady state analysis is performed to understand the hemodynamics at peak systole with inlet velocity of 0.93 m/s applied at inlet and at the outlets a constant pressure of 30 mmHg is applied [39]. The variation of diameter along the three branches of the carotid artery is calculated and a location where the diameter is minimum is located as indicated in Fig. 12. This is because the literature suggests that the assumption of blood as Newtonian fluid is valid in large arteries as the shear rates are higher. However, even in large arteries where there is stenosis leading to reduction in diameter this assumption does not hold since it masks the shear thinning character of blood [40].

At the location where the diameter is minimum, WSS is captured along the circumference of the ICA, and it can be seen in Fig. 13 that the Newtonian model overestimates the WSS in critical location [34,41]. High wall shear stress in an indicator of plaque rupture [42]. This is due to the assumption of constant viscosity by the Newtonian model at every location, but as blood is a shear thinning fluid the viscosity is highly dependent on the geometry and the applied boundary conditions.

Transient analysis is performed by applying the inlet velocity waveform as shown in Fig. 3 and outlet pressures as shown in Figs 4 and 5. Hemodynamic parameters like shear strain rate, WSS, velocity is

calculated along the axis of the carotid artery at 0.072 s where the velocity is maximum of 0.93 m/s. Figure 14 shows the variation of shear strain rate, velocity, WSS and diameter of CCA. As we can see there is no qualitative and significant quantitative difference between the Newtonian and Carreau-Yasuda blood viscosity models. But there is an increase in the value of WSS with the Newtonian model at plane 12 which is near the bifurcation and there will be flow recirculation and low WSS as can be seen clearly in the streamlines. The average diameter throughout the length of the CCA is 6.5 mm. Any artery above 6 mm in diameter is generally considered as large artery and we can also see from the plots that the shear rate is above 100 s^{-1}. Blood can be considered as Newtonian fluid for lumen diameter greater than 6 mm and also for shear rates above 100 s^{-1}, however, when there is flow circulation or reverse flows Newtonian models do not give correct results [39].

Similarly, even in the case of ECA there is no qualitative differences between the Newtonian and Carreau-Yasuda model. However, there is small overestimation of WSS in the CCA with the Newtonian model compared to the Carreau-Yasuda model as shown in Fig. 15. The average diameter of the ECA is 5 mm which can also be considered as a large artery, hence the Newtonian model will give satisfactory estimation of the hemodynamics. The average diameter of ICA is 4 mm. As shown in Fig. 14, the Newtonian model shows significantly higher values of shear strain rate when compared to the Carreau-Yasuda model at the location where the diameter is around 2 mm (i.e., at the neck of the stenosis shown in Fig. 12). This is the clear indicator of failure of the Newtonian model to accurately predict the hemodynamics at low diameter regions. In other locations where the diameter is higher there is not much difference between the two models.

4. Conclusions

It is observed that the influence of the shear thinning properties of blood on the hemodynamic parameters is not very significant in large arteries. Even in large arteries, at the region where there is low WSS leading to flow reversals and the region where the diameter is small due to stenosis the Newtonian model over exaggerates the hemodynamic parameters and does not predict the outcome accurately. It is observed by many researchers that the carotid sinus is the location where the plaque deposit occurs due to sudden enlargement of the lumen leading to flow recirculation. But, in the present study the stenosis is observed in the ICA. This is the clear indication that the plaque deposit is not only dependent on the changes in the lumen diameter and the flow recirculation region, but also on the other hemodynamic parameters and blood rheology. The Carreau-Yasuda model used in this study to capture the non-Newtonian properties of blood gives better approximations at critical locations. The limitations of this study is that the elasticity of the artery which is not incorporated, hence its effect on the hemodynamics is not shown. Further, the temporal variations of the parameters is not addressed along with the detailed rheological properties of blood.

References

[1] C.J. Moomaw, D. Woo, P. Khatri and S. Ferioli, Carotid arterystenosis as a cause of a stroke **40**(1) (2014), 36–41.
[2] D. Liepsch, A. Balasso, H. Berger and H.H. Eckstein, How local hemodynamics at the carotid bifurcation influence the development of carotid plaques, *Perspect Med* **1–12**(1) (2012), 132–136.
[3] A.M. Malek and S.L. Alper, Hemodynamic shear stress and its role in atherosclerosis **282**(21) (1999), 2035–2042.
[4] E. Cecchi et al., Role of hemodynamic shear stress in cardiovascular disease, *Atherosclerosis* **214**(2) (2011), 249–256.
[5] P.A. VanderLaan, C.A. Reardon and G.S. Getz, Site specificity of atherosclerosis: Site-selective responses to atherosclerotic modulators, *Arterioscler Thromb Vasc Biol* **24**(1) (2004), 12–22.

[6] C. Slager et al., The role of shear stress in the destabilization of vulnerable plaques and related therapeutic implications, *Nat Clin Pract Cardiovasc Med* **2**(9) (2005), 456–464.
[7] A.M. Shaaban and A.J. Duerinckx, Wall shear stress and early atherosclerosis: A review, *AJR Am J Roentgenol* **174**(6) (2000), 1657–1665.
[8] M. Cibis et al., Wall shear stress calculations based on 3D cine phase contrast MRI and computational fluid dynamics: A comparison study in healthy carotid arteries, *NMR Biomed* **27**(7) (2014), 826–834.
[9] F.J. Gijsen, F.N. van de Vosse and J.D. Janssen, The influence of the non-Newtonian properties of blood on the flow in large arteries: Steady flow in a carotid bifurcation model, *J Biomech* **32**(6) (1999), 601–608.
[10] G. Li, B. Chen and G. Zhou, Unsteady non-newtonian solver on unstructured grid for the simulation of blood flow, *Adv Mech Eng* **2013** (July 2013).
[11] C.K. Zarins et al., Carotid bifurcation atherosclerosis: Quantative correlation of plaque localization with flow velocity profiles and wall shear stress, *Circ Res* **53**(4) (1983), 502–514.
[12] B.K. Bharadvaj, R.F. Mabon and D.P. Giddens, Steady flow in a model of the human carotid bifurcation Part I-Flow visualization, *J Biomech* **15**(5) (1982), 349–362.
[13] D.H.K. Perktold, Numerical simulation of pulsatile flow in a carotid bifurcation model, *J Biomed Eng* **8** (1986), 193–199.
[14] D.B. Van de Vosse, F.N., J. Hart, Finite-element-based computational methods for cardiovascular fluid-structure interaction, *J Eng Math* **47** (2003), 335–368.
[15] K. Perktold and G. Rappitsch, Computer simulation of local blood flow and vessel mechanics in a compliant carotid artery bifurcation model **28**(7) (1995).
[16] J.S. Milner, J.A. Moore, B.K. Rutt and D.A. Steinman, Semodynamics of human carotid artery bifurcations: Computational studies with models reconstructed from magnetic resonance imaging of normal subjects, *J Vasc Surg* **28**(1) (1998), 143–156.
[17] C.A. Taylor, T.J.R. Hughes and C.K. Zarins, Finite element modeling of blood flow in arteries, *Comput Methods Appl Mech Eng* **158**(1–2) (1998), 155–196.
[18] V. Deplano and M. Siouffi, Experimental and numerical study of pulsatile flows through stenosis, *J Biomech* **32**(10) (1999), 1081–1090.
[19] D.A.S.H.M. Ladak and J.S. Milner, Rapid three dimensional segmentations of the carotid Bifurcation from serial MR images, *J Biomech Eng* **122**(10) (2000), 1814–1817.
[20] D.A. Steinman, T.L. Poepping, M. Tambasco, R.N. Rankin and D.W. Holdsworth, Flow patterns at the stenosed carotid bifurcation: Effect of concentric versus eccentric stenosis, *Ann Biomed Eng* **28**(4) (2000), 415–423.
[21] Q. Long, X.Y. Xu, K.V Ramnarine and P. Hoskins, Numerical investigation of physiologically realistic pulsatile flow through arterial stenosis **34** (2001), 1229–1242.
[22] J.S. Stroud, S.A Berger and D. Saloner, Fumerical analysis of flow through a severely stenotic carotid artery bifurcation, *J Biomech Eng* **124**(1) (2002), 9–20.
[23] I. Marshall, S. Zhao, P. Papathanasopoulou, P. Hoskins and X.Y. Xu, MRI and CFD studies of pulsatile flow in healthy and stenosed carotid bifurcation models, *J Biomech* **37**(5) (2004), 679–687.
[24] S.Z. Zhao, P. Papathanasopoulou, Q. Long, I. Marshall and X.Y. Xu, Comparative study of magnetic resonance imaging and image-based computational fluid dynamics for quantification of pulsatile flow in a carotid bifurcation phantom, *Ann Biomed Eng* **31**(8) (2003), 962–971.
[25] U. Morbiducci et al., Outflow conditions for image-based hemodynamic models of the carotid bifurcation: Implications for indicators of abnormal flow, *J Biomech Eng* **132**(9) (2010), 091005.
[26] Y. Fan, W. Jiang, Y. Zou, J. Li, J. Chen and X. Deng, Numerical simulation of pulsatile non-newtonian flow in the carotid artery bifurcation, *Acta Mesh Sin* **25**(2) (2009), 249–255.
[27] B.M. Johnston, P.R. Johnston, S. Corney and D. Kilpatrick, Non-newtonian blood flow in human right coronary arteries: Steady state simulations, *J Biomech* **37**(5) (2004), 709–720.
[28] J. Chen and X.Y. Lu, Numerical investigation of the non-Newtonian blood flow in a bifurcation model with a non-planar branch, *J Biomech* **37**(12) (2004), 1899–1911.
[29] F.J. Gijsen, E. Allanic, F.N. van de Vosse and J.D. Janssen, The influence of the non-newtonian properties of blood on the flow in large arteries: unsteady flow in a 90 degrees curved tube, *J Biomech* **32**(7) (1999), 705–713.
[30] S.S. Shibeshi and W.E. Collins, The rheology of blood flow in a branched arterial system, *Appl Rheol* **15**(6) (2005), 398–405.
[31] B.M. Johnston, P.R. Johnston, S. Corney and D. Kilpatrick, Non-newtonian blood flow in human right coronary arteries: Steady state simulations, *J Biomech* **37**(5) (2004).
[32] C.A.J. Fletcher, *Computational Techniques for Fluid Dynamics 1* 2nd ed. Springer-Verlag Berlin Heidelberg, (1998).
[33] H. Gharahi, B.A. Zambrano, D.C. Zhu, J.K. Demarco and S. Baek, Computational fluid dynamic simulation of human carotid artery bifurcation based on anatomy and volumetric blood flow rate measured with magnetic resonance imaging, *Int J Adv Eng Sci Appl Math* **8**(1) (2016), 46–60.

[34] Y.I. Cho and K.R. Kensey, Effects of the non-newtonian viscosity of blood on flows in a diseased arterial vessel. Part 1: Steady flows, *Biorheology* **28**(3–4) (1991), 241–262.
[35] M.S. Olufsen, Structured tree outflow condition for blood flow in larger systemic arteries, *Am J Physiol* **276**(1 Pt 2) (Jan 1999), H257–268.
[36] M.S. Olufsen, C.S. Peskin, W.Y. Kim, E.M. Pedersen, A. Nadim and J. Larsen, Numerical simulation and experimental validation of blood flow in arteries with structured-tree outflow conditions, *Ann Biomed Eng* **28**(11) (2000), 1281–1299.
[37] S. Chandra and A. Garcı, Impedance-based outflow boundary conditions for human carotid haemodynamics, *Computer Methods in Biomechanics and Biomedical Engineering* **17**(11) (February 2013), 1248–1260.
[38] E. Shaik, Numerical simulations of blood flow In arteries using fluid-structure interactions, *PhD Thesis* (2007).
[39] Y. Ohhara et al., Investigation of blood flow in the external carotid artery and its branches with a new 0D peripheral model, *Biomed Eng Online* (2016), 1–17.
[40] D.A. Steinman, Assumptions in modelling of large artery hemodynamics, in: *Modelling of Physiological Flows* Springer Milan Dordrecht Heidelberg London NewYork, (2012), 10–13.
[41] J. Xiang, M. Tremmel, J. Kolega, E.I. Levy, S.K. Natarajan and H. Meng, Newtonian viscosity model could overestimate wall shear stress in intracranial aneurysm domes and underestimate rupture risk, *Journal of Neurointerventional Surgery* **4**(5) (2011), 351–357.
[42] Z. Teng and P.K. Woodard, 3D critical plaque wall stress is a better predictor of carotid plaque rupture sites than flow shear stress: An in vivo MRI-based 3D FSI study *J Biomech Eng* **132**(3) (Mar 2010), 031007.